Poly(*N*-vinylpyrrolidone) anti-malaria conjugates of membrane disruptive peptides.

Simbarashe Jokonya [†], *Marvin Langlais* [†], *Meta Leshabane*[§], *Paul W Reader* [†], *Johan A Vosloo* [‡], *Rueben Pfukwa* [†], *Dina Coertzen*[§], *Lyn-Marie Birkholtz*[§], *Marina Rautenbach*[‡]* *and Bert Klumperman*[†]*

[†] Department of Chemistry and Polymer Science, Stellenbosch University, Private Bag X1, Matieland 7602, South Africa.

[‡] BioPep[TM] Peptide Group, Department of Biochemistry, Stellenbosch University, Private Bag X1, Matieland 7602, South Africa.

[§] Department of Biochemistry, Genetics and Microbiology, Institute of Sustainable Malaria Control, University of Pretoria, Private Bag X20, Hatfield 0028, South Africa.

KEYWORDS: Poly(*N*-vinylpyrrolidone), tyrocidine, bioconjugates, self-assembly, erythrocytes, malaria.

ABSTRACT

The concepts of polymer-peptide conjugation and self-assembly were applied to antimicrobial peptides (AMPs) in the development of a targeted anti-malaria drug delivery construct. This study describes the synthesis of α-acetal, ω-xanthate heterotelechelic poly(*N*-vinylpyrrolidone) (PVP) via reversible addition-fragmentation chain-transfer (RAFT) mediated polymerization, followed by post-polymerization deprotection to yield α-aldehyde, ω-thiol heterotelechelic

PVP. A specific targeting peptide, GSRSKGT, for *Plasmodium falciparum* infected erythrocytes was used to sparsely decorate the α-chain ends via reductive amination whilst cyclic decapeptides from the tyrocidine group were conjugated to the ω-chain end via thiol-ene Michael addition. The resultant constructs were self-assembled into micellar nano-aggregates whose sizes and morphologies were determined by dynamic light scattering (DLS) and transmission electron microscopy (TEM). The *in vitro* activity and selectivity of the conjugates were evaluated against intraerythrocytic *P. falciparum* parasites.

INTRODUCTION

Malaria is the most prevalent parasitic disease and one of the leading causes of death of children under the age of 5.[1, 2] The majority of malaria infections occur in tropical areas and are caused by several species of protozoan parasites belonging to the genus *Plasmodium.* The five *Plasmodium* species, *P. ovale*, *P. malariae*, *P. vivax, P. falciparum* and *P. knowlesi* are transmitted to humans by the female *Anopheles* mosquito.[3, 4] *P. falciparum* is responsible for the majority of deaths, > 95% of which are prevalent in sub-Saharan Africa, mainly affecting pregnant women and children under the age of 5.[1, 2] Several classes of antimalarial drugs have been developed to treat malaria, including the quinolines, antifolates and artemisinins. However, resistance of malaria parasites to these drugs is now rolling back these successes.[5, 6] Therefore, there is need to develop new and effective malaria treatment regimes.

Antimicrobial peptides (AMPs), which form part of the an ancient innate defence system that can be found in the animal, plant and microbial kingdoms in the fight against invasive bacteria, fungi, viruses and protozoa, are gaining interest as therapeutic agents for several pathogens.[7, 8] AMPs as a group have diverse structures and vary in size from about 800 - 8000 kDa. AMPs, however, share a number of characteristics with the most important being their amphipathic nature and high isoelectric points (pI) which facilitate selective electrostatic

interactions with target membrane lipids.[9-12] An interesting example of the AMP complex called tyrothricin produced non-ribosomally by *Brevibacillus parabrevis*, previously known as *Bacillus brevis*.[13, 14] The peptides found in the tyrothicin complex consist of up to 28 different cationic cyclic decapeptides from the tyrocidine (Trc), tryptocidine (Tpc) and phenycidine groups, as well as up to nine neutral pentadecapeptides called the gramicidins.[13, 14] Both the cyclic decapeptide group and gramicidins have been shown to be active against the erythrocyte stage of *P. falciparum*.[15] Rautenbach *et al*.[15] reported that gramicidin S, an analogous cyclic decapeptide that shares the Val-Orn-Leu-D-Phe-Pro pentapeptide moiety with the Trcs, was less active and less selective for erythrocyte stage *P. falciparum* when compared to Trc. Furthermore, gramicidin S was shown to exert its low micromolar parasitic inhibition by rapid lysis of infected erythrocytes, whilst Trc, on the other hand, did not result in overt lysis of infected erythrocytes but also facilitated selective parasite death at nanomolar concentrations via a mechanism of parasite development inhibition. From these studies and a follow-up study by Leussa,[16] it was hypothesized that the low nanomolar anti-plasmodium activity of the tyrocidines is related to sensitive intracellular targets, possibly with multiple modes of action. To limit the development of resistance by microbial pathogens including *P. falciparum*, rapid activity, multiple targets and modes of action in the same drug system or formulation would be the ideal approach.[17] The action of Trc on *P. falciparum* does match these criteria, apart from that it could be cytotoxic at micromolar dosages, therefore, if these peptides are to be used against *P. falciparum*, they must be modified to limit toxicity or be contained within a drug delivery system.

Despite considerable research efforts being channelled towards the identification of potent and selective peptides, the drug delivery aspects of AMPs have largely remained untouched.[18] For therapeutic applications, it might be essential to combine Trc with a drug delivery system so as to not only circumvent their toxic nature towards healthy cells, but also

to prevent cell-mediated immune responses due to cellular damage. The proteolytic susceptibility of most AMPs can lead to degradation and loss of activity when parenterally administered. However, the cyclic nature of the Trcs and D-amino acid residues in the structure will allow for better systemic stability, specifically protease-related stability, compared to linear and all L-residue AMPs.[19, 20] The cationic and amphipathic nature of AMPs, including Trc, could pose a problem when administered systemically, as their inherent chemistry facilitates their binding to serum proteins such as albumin causing subsequent clearance from blood circulation.[21-23] Polymer-peptide conjugation is a known approach for improving the efficacy of pharmaceuticals, including peptides, by reducing proteolytic degradation, increasing blood circulation time, preventing uptake by the reticular endothelial system and reducing cytotoxicity.[24] Despite that cyclic Trcs, containing non-protein residues and D-amino acids are considerably less susceptible to proteolytic degradation[19, 20], conjugation to polymers will likely further reduce the vulnerability. The main aim of the Trc-polymer conjugation, however, is to potentially diminish and localise the toxicity of Trcs, which are toxic on their own.

Polymer-peptide conjugates can be synthesized by growing a polymer chain from a suitably functionalized peptide (grafting-from), or by coupling a ready-made polymer to a peptide (grafting-to).[25-27] Both approaches benefit from controlled chain growth polymerization techniques, which produce well-defined polymers with predictable molar masses (M_n), low dispersity ($Đ$) and precisely placed and known functional handles.[28] Polyethylene glycol (PEG) is the preeminent polymer for conjugating to peptides, via grafting-onto approach. PEG is readily prepared by living anionic polymerization of ethylene oxide, and is easily end-functionalized.[29]

In the last two decades, the advent of reversible deactivation radical polymerization techniques (RDRP) has expanded the scope of accessible, well-defined biocompatible

synthetic polymers with predictable M_n, low $Đ$ and precise functionalities.[30, 31] Moreover RDRP methods, in particular the reversible addition-fragmentation chain-transfer (RAFT) process, are more robust than anionic polymerization and tolerate a wide range of functional groups and experimental conditions. Other complimentary advances in materials science include the use of dynamic covalent chemistry, which enables stimuli responsiveness[32] and increased understanding of self-assembly,[33] in particular that of polymer- peptide systems, enhancing the possibilities of harnessing the potential of AMPs such as the Trcs.

In this study we investigated the potential of poly(*N*-vinylpyrrolidone)-Trc (PVP-Trc) conjugate drug delivery system in anti-malarial therapy. PVP is a well-known biocompatible polymer, with numerous applications in the beverage industry, in cosmetics and in pharmaceuticals. It is readily synthesized via RAFT polymerization, and easily end-functionalized with bio-relevant end groups such as thiols and aldehydes. Heterotelechelic α-aldehyde, ω-thiol-PVP was prepared via the RAFT process and subsequently chain-end deprotected based on our previous work.[34] Thiol-ene Michael addition chemistry on the ω-end group was employed to conjugate a prepared acrylate functionalized Trc, whilst the α-aldehyde end-group was used to attach a malaria infected erythrocyte-specific targeting ligand. Subsequently, the conjugates were self-assembled into core (Trc) - shell (PVP) spherical morphologies in aqueous solutions before evaluating the haemolytic toxicity and efficacy of these drug delivery vehicles against erythrocytes infected with the malaria parasite, *P. falciparum.*

EXPERIMENTAL SECTION

Materials. Acryloyl chloride (> 97%), *tert*-butyl hydroperoxide (70 wt.% in water), But-3-yn-2-ol (≥ 97%), 3-chloropropionylaldehyde (≥ 90%), copper(II) sulfate pentahydrate (≥ 98%), *N*,*N*-diisopropylethylamine (DIPEA, 99.5%), DMSO-d_6 (99.9% atom D), HCl (4M in

dioxane), *n*-hexylamine (99%), potassium ethyl xanthogenate (≥ 96%), *n*-propylamine (98%), pyrene (98%), 6-aminofluorescein (≥ 95%) sodium ascorbate (≥ 98%), sodium azide (NaN_3, ≥ 99%), lithium bromide (LiBr, ≥ 99%), sodium borohydride ($NaBH_4$, > 95%), sodium cyanoborohydride ($NaBH_3CN$, > 95%), *p*-toluenesulfonyl chloride (≥ 98%), triethylamine (≥ 99%) and *N*-vinylpyrrolidone (NVP), all Sigma Aldrich, were used as received. Sodium sulphite (Na_2SO_3, 96%) was purchased from Riedel-de Haën. GSRSKGT (≥ 99% GL Shanghai).

Ethics. All *in vitro* experiments were carried out at the University of Pretoria with ethics approvals from the Faculty of Natural and Agricultural Sciences (ref: 180000094) for the cultivation of malaria parasites and the Faculty of Health Sciences (ref 506/2018) for the use of human erythrocytes to this end.

Methods. *Nuclear Magnetic Resonance (NMR) Spectroscopy.* ^{1}H and ^{13}C NMR spectra were recorded on a Varian VXR-Unity 400 MHz spectrometer, in deuterated solvents, at 25 °C. Chemical shifts are reported in parts per million (ppm), downfield of tetramethylsilane, referenced to residual solvent peaks. Coupling constants are reported in Hertz (Hz), and resonance multiplicities are described as s (singlet), d (doublet), t (triplet), q (quartet) or m (multiplet).

Size Exclusion Chromatography (SEC). SEC was carried out on an Agilent 1260 HPLC instrument (Agilent Technologies, Waldbronn, Germany) comprising the following: autosampler, on-line degasser, quaternary pump unit and a thermostatic column compartment set to 40 °C. The detectors used were an Agilent VWD ultraviolet (UV) detector at a UV wavelength of 290 nm and an RI detector at 40 °C. Three GRAM columns (PSS Polymer Standards Service, GmbH, Mainz, Germany) with polyester copolymer as a stationary phase and 10 μm particle size and porosities of either 100 Å and 3 000 Å were used in tandem. A

guard column with the same packing material was used. The eluent system used was *N*,*N*-dimethylformamide (HPLC grade with 0.05% w/v LiBr salt) at a flow rate of 0.8 $mL \cdot min^{-1}$. Calibration was carried out using low dispersity poly(methyl methacrylate) (Polymer Standards Service (PSS), Mainz, Germany) with peak maximum molecular weights (M_p) ranging between 800 $g \cdot mol^{-1}$ and 2 200 000 $g \cdot mol^{-1}$. Therefore, the SEC data obtained are reported as PMMA equivalents. PSS WinGPC Unichrom 8.2 software was used to acquire and process the data.

Ultra-performance liquid chromatography in tandem with electrospray mass spectroscopy (UPLC-MS). UPLC-MS was conducted utilising a Waters Acquity Ultra Performance Liquid Chromatograph coupled to a Waters Synapt G2 high resolution mass spectrometer fitted with a Z-spray electrospray ionisation source. For direct injection ESMS and UPLC-MS analyses, 1-3 µL of the sample solution (± 50 ng Trc or modified Trc in 50% acetonitrile) was injected each time and subjected to a capillary voltage of 3.0 kV, source voltage of 15 V and temperature of 120 °C. Collision energies in the trap and transfer collision cell was kept at 4 eV and 0 eV respectively. A desolvation gas (N_2) flow was maintained at of 650 L/h and desolvation temperature was at 275 ºC. Mass spectral data were collected in positive mode by continuum scanning over an *m/z* range of 300-2000. For the UPLC analysis of the Trcs and modified Trcs, we employed an Acquity UPLC® BEH C_{18} column (2.1 × 50 mm, 1.7 µm spherical particles, Millipore-Waters, La Jolla, USA). Chromatographic separation was accomplished by the use 0.1% formic acid (A) to acetonitrile (B) gradient (100% A for 30 seconds, 0 to 30% B from 30 to 60 seconds, 30 to 60% B from 1 to 10 minutes, 60 to 80% B from 10 to 15 minutes at a flow rate of 300 µL/min), followed by re-equilibration of the column to initial conditions.

Dynamic Light Scattering (DLS). DLS was performed on a Malvern Instruments ZetaSizer Nano series (Worcestershire, U.K) 1000HSa equipped with a He-Ne laser operating at a wavelength of 633 nm. The scattered light was detected offline at an angle of 175 °. The particle

size and distribution were obtained from 3 measurements, each comprising 10 runs. The particle size and distribution were determined using CONTIN analysis and presented as the Z-average particle size.

Transmission Electron Microscopy (TEM). Samples were imaged using the Tecnai 20 transmission electron microscope (TEM) (Thermo Fisher (formerly FEI), Eindhoven, Netherlands) fitted with a LaB_6 emitter and operating at 200 kV and a Gatan Tridiem 863 UHS (Gatan, UK). The images were collected using the embedded Gatan CCD camera (2048 × 2048 pixels). Sample preparation was done on plasma treated copper grids.

Fluorescence spectroscopy. The fluorescence excitation spectra of pyrene were measured at varying block copolymer concentrations using a Perkin Elmer Luminescence LS50B spectrometer using FL Winlab version 4.0 for data processing.

Thermodynamic stability. A dilution series PVP_{4K}-Trc and PVP_{9K}-Trc conjugates was prepared in PBS at concentrations ranging from 0.1 $\mu g \cdot mL^{-1}$ to 1 $mg \cdot mL^{-1}$, each made up to a final volume of 4.5 mL. Subsequently, a stock solution of pyrene dissolved in acetone (36.4 mg/mL, 1.8×10^{-4} M) was prepared and cooled to 4 °C. From the pyrene solution, 15 µL was pipetted into each conjugate dilution to make up a final pyrene concentration of 6.0×10^{-7} M. The prepared conjugate dilutions were left for 24 h at 25 °C in the dark to facilitate the partitioning of pyrene into the core segments of the conjugates. The fluorescence excitation spectra were recorded from 300 to 360 nm with the emission wavelength at 390 nm. The spectra were recorded at a scan rate of 250 $nm \cdot min^{-1}$ and the intensity ratio of I_{337nm}/I_{333nm} was plotted against the logarithm of the conjugate concentration to determine the CMC.

In vitro cultivation of asexual P. falciparum parasites and antimalarial assays. Drug sensitive *P. falciparum* parasites (NF54 strain obtained from BEI resources) were cultured *in vitro* at 5%

haematocrit in human type O/A Rhesus positive erythrocytes (from healthy volunteer donors, University of Pretoria Health Sciences Ethics approval 506/2018) suspended in complete culture medium (RPMI-1640 medium (Sigma-Aldrich) supplemented with 25 mM HEPES, 2% (w/v) D-glucose, 200 μM hypoxanthine, 23.8 mM sodium bicarbonate, 0.5% AlbuMAX II (Sigma-Aldrich) and 24 $\mu g \cdot mL^{-1}$ gentamycin (Fresenius, Germany). The parasite cultures were maintained at 37 °C under hypoxic conditions (90% N_2, 5% O_2, and 5% CO_2) and synchronised with D-sorbitol (5%).[35] The SYBR green I fluorescence assay was used to determine proliferation of conjugate treated parasites (1% haematocrit, 1% parasitaemia) which were incubated for 96 h under hypoxic conditions at 37 °C. Chloroquine disulphate (1 μM) was the positive control whilst complete untreated parasites was the negative control for inhibition of proliferation.[35] At the conclusion of the 96 h growth incubation period, equal volumes of the *P. falciparum* parasite cultures and SYBR Green I lysis buffer [0.2 μL/mL 10 000× SYBR Green I; 20 mM Tris, pH 7.5; 5 mM EDTA; 0.008% (*w/v*) saponin; 0.08% (*v/v*) Triton X-100] were transferred to new 96-well plates. The samples were incubated at 37 °C for 1 h after which fluorescence was measured with a GloMax®-Explorer Detection System with Instinct® Software (excitation at 485 nm and emission at 538 nm). Dose-response curves were plotted using GraphPad v6.0. from which half-maximal inhibitory concentrations (IC_{50}) were obtained. Experiments were performed in technical triplicate for three independent biological replicates.

Human erythrocyte haemolysis assays. Human whole blood (type O or A Rh-positive erythrocytes) was collected in anticoagulated blood bags (Adcock Ingram) from consenting donors. The blood was washed thrice with phosphate buffered saline [1 × PBS: 137 mM NaCl (Merck, USA), 2.7 mM KCl (Merck, USA), 10 mM KH_2PO_4 (Merck, USA), pH 7.4] and thereafter centrifuged at 3000 × *g* to remove serum and buffy coat. Erythrocytes (4% haematocrit) were exposed to varying conjugate concentrations in 96 well plates for 48 h at 37 °C. Untreated erythrocytes and erythrocytes treated with Triton-X were employed as negative

(0% haemolysis) and positive controls (100% haemolysis) respectively. Following incubation, erythrocyte suspensions were centrifuged at 3000 × *g* for 3 min. The amount of released haemoglobin in the supernatant (3:7 dilution) was measured by absorbance at 540 nm (Multiskan Ascent V1.24, Thermo Labsystems). Dose-response curves were drawn in Graphpad Prism v6.0. and half-maximal haemolytic concentrations (HC_{50}) obtained Data are representative of technical triplicates for three independent biological repeats.[36]

Cytotoxicity. HepG2 cells were grown in DMEM with FBS (10%) and penicillin/streptomycin (1%) at 37 °C (CO2 (5%), 90% humidity). The media was changed every 2 days as needed depending on the cell confluency, which was monitored using a phase contrast microscope (40× magnification). Cells were passaged at 70 – 80% monolayer confluency using 1x Trypsin-EDTA (Sigma-Aldrich). The cell viability was monitored microscopically with Trypan-Blue (0.2%). Approximately 100 000 cells/well were plated in 96-well plates and the cells were grown for 24 h at 37 °C. After this time, the cells were treated with each compound (10 and 2 M) for 48 h at 37 °C (CO2 (5%)). PBS (40 µL) was used to dilute the supernatant (60 µL) which was added to new 96-well plates. The cytotoxicity was determined using the CytoSelect™ lactate dehydrogenase (LDH) cytotoxicity assay kit. DMEM complete culture media was used as the background control. Untreated viable cells and cells treated with Triton-X 100 (dead cells) were used as the negative and positive control for cytotoxicity, respectively. Emetine was used as a reference control. Equation 1 was used to calculate the cytotoxicity where OD is the absorbance at 450 nm determined using a UV-Vis spectrometer, T is drug treated HepG2 cells, P is the positive control and N is the negative control. Experiments were performed in technical triplicate for three independent biological repeats (n = 3).

$$Cytotoxicity = \frac{OD_T - OD_N}{OD_p - OD_N} \times 100 \qquad \text{(Equation 1)}$$

Light and confocal fluorescence microscopy. Blood smears were prepared at various incubation times for examination by light and fluorescence microscopy. Slides prepared for light microscopy were stained with Giemsa. Fluorescence based imaging was performed on Carl Zeiss (Germany) LSM780 with ELYRA S.1 confocal microscope. Images were acquired using a 10× air immersion objective (EC "Plan-Neofluar"10×/0.3 M27) and 60× oil immersion objective (Olympus Plan APO N 60×/1.42 Oil/0.17/FN26.5). A diode 405 nm and an argon multi-line laser 25 mW at 488 nm and 561 nm laser were used as a light source and the fluorescence intensity was measured using a GaAsP detector. Laser power and master gain were chosen for 488 nm (fluorescein) to achieve an optimal signal/noise ratio with minimal pixel saturation.

Synthesis. *S-(but-3-yn-2-yl) O-ethyl carbonodithioate (1)* was synthesized as described in literature.[34]

Synthesis of 3-azido-1,1-diethoxypropane (2). 3-chloropropionaldehyde diethyl acetal (10 g, 60.3 mmol) was diluted in dimethyl sulfoxide (60 mL), followed by portion wise addition of sodium azide (9.75 g, 150.5 mmol), before stirring the reaction at 50 °C for 16 h. Thereafter, the reaction mixture was poured into water (50 mL) and extracted into ethyl acetate (3 × 40 mL), before washing the organic phase with brine (2 × 20 mL), and then with deionized water (2 × 20 mL). The organic phase was dried over $MgSO_4$ and concentrated under reduced pressure, yielding the product as an orange oil (9.35 g, 90%). ^{1}H NMR (400 MHz, 298 K, $CDCl_3$) δ (ppm) = 4.61-4.58 (t, *J* = 5.6 Hz, 1H), 3.70-3.63 (dq, *J* = 9.4, 7.1 Hz, 2H), 3.54-3.47 (dq, *J* = 9.4, 7.0 Hz, 2H), 3.39-3.35 (t, *J* = 6.8 Hz, 2H), 1.90-1.85 (td, *J* = 6.8, 5.7 Hz, 2H), 1.22-1.19 (t, *J* = 7.0 Hz, 6H). ^{13}C NMR (100 MHz, 298 K, $CDCl_3$) δ (ppm) = 100.4, 61.8, 47.5, 33.2, 15.3.

Synthesis of S-(1-(1-(3,3-diethoxypropyl)-1H-1,2,3-triazol-4-yl)ethyl) O-ethyl carbonodithioate (XA1) was prepared as described in literature.[34]

Synthesis of α-acetal, ω-xanthate heterotelechelic PVP. In a typical procedure, NVP (6 g, 53.0 mmol), xanthate (XA1) (125 mg, 0.360 mmol) and *tert*-butyl hydroperoxide (8.11 mg, 0.090 mmol) were weighed into a Schlenk tube and dissolved in pH 7.4 PBS buffer solution (5.5 mL). The solution was degassed by bubbling argon gas for 20 min. Na_2SO_3 (11.3 mg, 0.090 mmol) was separately dissolved in pH 7.4 PBS (0.5 mL) and degassed by bubbling argon for 10 min. The Na_2SO_3 solution was added to the monomer solution using a degassed syringe, to start the polymerization, which proceeded at room temperature for 16 h. Thereafter, an aliquot of the reaction mixture (~ 20 mg) was withdrawn to determine conversion by ^{1}H NMR spectroscopy in D_2O, whilst the rest of the sample was lyophilized. Afterwards, the polymer was dissolved in minimum $CHCl_3$ and precipitated from diethyl ether, three times, dried under vacuum and analyzed by NMR spectroscopy and SEC.

Synthesis of α-aldehyde, ω-thiol PVP via a one pot sequential chain end deprotection. In a typical procedure, *n*-hexylamine (15 equiv., 2.25 g, 23 mmol) was added to a solution of α-acetal, ω-xanthate PVP (4000 g·mol^{-1}, 6 g, 1.5 mmol) in acetone (40 mL), and the mixture stirred at room temperature for 4 h. Thereafter, 4 M solution of HCl in dioxane (13.5 mL) was added, bringing the HCl concentration to 1 M, and the reaction was stirred at room temperature for 4 h. The solution was purified by dialysis (2000 Da MWCO) against MeOH/H_2O (1:1) for 2 days and deionised water for one day and lyophilized, yielding α-aldehyde, ω-thiol heterotelechelic PVP as a white powder (1.24 g, 55%) before analysis by ^{1}H NMR spectroscopy and SEC.

Synthesis of tyrocidine acrylate (Trc acrylate). Trc was produced utilising *B. parabrevis* as described by Vosloo *et al*.[37] The gramicidins were removed from dried crude extract containing

the Trc by multiple precipitation steps utilising ether:acetone (1:1, v/v). The insoluble precipitate containing the Trcs was collected and lyophilised. The collected Trc fractions were analysed utilising UPLC-MS to ensure that it was gramicidin free and of high purity. To modify the Trcs with acrylate, a 50 mL round bottom flask was charged with Trc (225 mg, ± 0.17 mmol), DMF (30 mL) and DIPEA (600 μL, 3.46 mmol), and the solution was chilled in an ice bath, before adding a solution of acryloyl chloride (28 μL, 0.346 mmol), in chilled DMF (5 mL), dropwise. The reaction warmed up to room temperature on its own before being stirred for 48 h. DMF was evaporated under reduced pressure, the resultant solid dissolved in minimal ethanol and precipitated from diethyl ether, five times. The sample was then dried under a stream of nitrogen, dissolved in 1:1 (v/v) ACN/H_2O (30 mL), before lyophilization, yielding the product as a light brown powder (215 mg, 92%), which was subsequently analysed by UPLC-MS.

Synthesis of α-GSRSKGT, ω-thiol PVP via reductive amination. In a typical procedure, α-aldehyde, ω-thiol PVP (4000 g·mol^{-1}, 120 mg, 30 μmol) was dissolved in sodium borate solution (SBS, 2 mL, pH 9.7). $NaBH_3CN$ (10 equiv.) and GSRSKGT (0.41 mg, 0.6 mmol) were separately dissolved in SBS buffer (1 mL and 0.5 mL, respectively) and subsequently added to the polymer solution. The reaction mixture was stirred at room temperature, overnight, before adding 10 times excess *n*-propylamine, to passivate the remaining aldehyde functionalities and stirred for 6 h, before being dialysed (3500 Da MWCO) against deionised water, for 24 h. Finally, the product was isolated by lyophilisation, and obtained as a white powder.

Synthesis of α-GSRSKGT, ω-tyrocidine PVP bioconjugate via nucleophile thiol-ene Michael addition. In a typical procedure, α-GSRSKGT, ω-thiol PVP (4000 g·mol^{-1}, 20 mg, 5 μmol) and $NaBH_4$ (2.00 mg, 0.050 mmol) were dissolved in DMF (2 mL) and the solution was degassed

by purging with argon for 5 min. Trc acrylate (8.57 mg, 6.2 μmol) was dissolved in DMF (1 mL) and added to the PVP solution. DIPEA (4 μL, 0.030 mmol) was added and the reaction was stirred at room temperature for 48 h. The solution was purified via dialysis (2000 Da MWCO) against EtOH/H_2O (1:1 v/v) for 24 h, and pure H_2O for a further 24 h, before lyophilizing, yielding the product, α-GSRSKGT, ω-tyrocidine PVP bioconjugate as a white powder (18 mg, 68%), which was characterized by ^{1}H NMR spectroscopy.

RESULTS AND DISCUSSION

In the first part of the study, the self-assembly properties of the PVP-tyrocidine resultant conjugates in aqueous media were studied. In the second part of the study, activity of the bioconjugates as anti-malarial agents, as well as the specificity for conjugates bearing a ligand proposed to be selective for infected erythrocytes, were evaluated as a function of the inhibitory concentration and haemolytic concentration. For the purposes of this discussion, we employ the term "Trc" to refer to the purified peptide preparation consisiting of mainly tyrocidine analogues (72.1% of Trcs), a smaller fraction of tryptocidine (19.5% of Tpc), with the rest made up by other cyclic decapeptides (6.8)% and VGA (1.6%) (Refer to Table S2 and Fig S9 in supplementary data).

Synthesis of α-aldehyde, ω-thiol heterotelechelic PVP via RAFT/MADIX polymerization. Biocompatible polymers with orthogonally addressable end-functionalities, such as aldehydes and thiols, have many applications in bioconjugate formation.[28, 38] RAFT polymerization is a mature technology for preparing such α,ω-heterotelechelic biocompatible polymers.[28, 38] PVP, an established biocompatible polymer is readily accessible via the RAFT polymerization of NVP, using functional xanthate chain transfer agents in either organic or aqueous media.[39-41]

Towards the preparation of α-aldehyde, ω-thiol PVP based on our earlier work,[34, 42] we first synthesized a triazole based xanthate RAFT agent bearing an acetal protected aldehyde functionality in the R-group (Scheme 1 (A)) and the structure was verified by NMR spectroscopy (Figures S1 and S2). Thereafter, we used this RAFT agent to mediate the aqueous RAFT polymerization of NVP (Scheme 1 (B)) in aqueous media, *i.e.* PBS buffer, pH 7.5, using the redox initiation pair *tert*-butyl hydroperoxide and sodium sulphite, at room temperature, based on conditions reported by Destarac *et al.*[43]

Two degrees of polymerization (DP_n) were targeted (DP_n = 44 and 88). Polymerizations proceeded to high conversions, > 80%, and SEC analysis revealed good control over molar mass, and low $Đ$ (Table 1). ^{1}H NMR spectroscopy analysis confirmed the retention of RAFT end-groups (Figure S3 (A)), with the α-acetal signals (methylenes 'h' and 'i' at 4.28 ppm and 4.47 ppm, respectively) and ω-xanthate signals (methylene 'f' at 4.62 ppm). M_n values calculated from ^{1}H NMR spectroscopy were also in good agreement with theoretical M_n values, indicating good end-group retention (Table 1). Finally we accessed α-aldehyde, ω-thiol PVP, via our earlier reported one-pot, two-step end-group deprotection procedure (Scheme 1 (B)).[44] First, the ω-xanthate end-group was aminolysed using *n*-hexylamine, before lowering the pH, using HCl in dioxane, resulting in the quaternisation of excess hexylamine and deprotection of the acetal functionality, into an aldehyde.

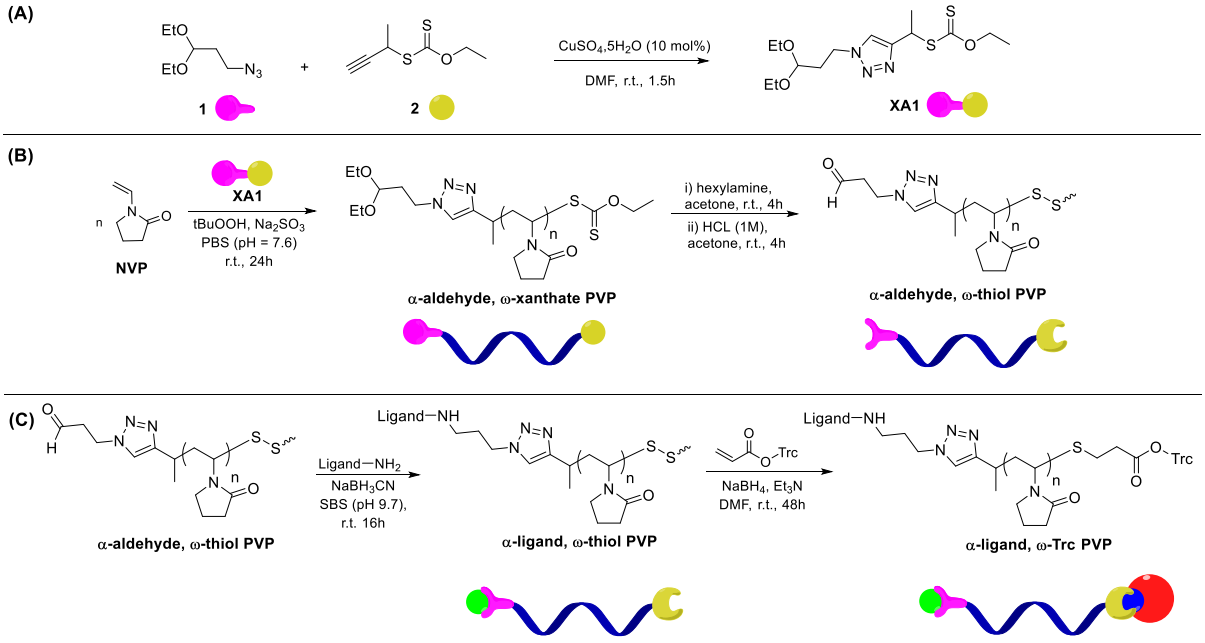

Scheme 1. (A) Synthetic procedure for the synthesis of the xanthate XA1. (B) Synthetic procedure for the synthesis α-aldehyde, ω-thiol PVP using RAFT/MADIX polymerization and one-pot sequential end chain deprotection. (C) Post-polymerization modification introduced a targeting group (α-chain end) via reductive amination followed by subsequent synthesis of PVP-Trc conjugates via nucleophilic thiol-ene Michael addition.

Table 1. Summary of the experimental and theoretical size parameters for the RAFT mediated polymerization of NVP using XA1 as CTA.

Samples	Conv[a] (%)	$M_{n\ (theo)}$[b] (g·mol^{-1})	$M_{n\ (NMR)}$[a] (g·mol^{-1})	$M_{n\ (SEC)}$[c] (g·mol^{-1})	$Đ^c$
PVP_{4K}	83	4150	3300	4000	1.30
PVP_{9K}	87	8700	8400	9300	1.25

[a]Determined by ^{1}H NMR in $CDCl_3$. [b]$M_{n(theo)} = ([monomer]_0 \times conv. \times M_{monomer})/[CTA]_0 + M_{CTA}$; [CTA]/[Initiator] = 4:1 ratio. [c]Determined by SEC analysis in DMF + LiBr (PMMA as standards).

^{1}H NMR analysis of the purified polymer confirmed the removal of the ω-xanthate end-group, by the disappearance of the methylene signal 'f', as well as the deprotection of acetal into aldehyde functionality by the appearance of the aldehyde proton 'j' at 9.7 ppm (Figure S3 (B)). SEC analysis of the end-modified polymers revealed a broadening of the molar mass distribution in the RI traces of the end-modified samples (Figure S4), which is attributable to oxidative coupling of ω-thiol chain ends, forming disulphides, as illustrated in Scheme 1, effectively doubling the polymer M_n.

Synthesis of PVP-Tyrocidine conjugates with malaria targeting ligand. Our strategy for preparing the polymer-peptide conjugates entails introduction of a targeting ligand specific for infected erythrocytes to the α end-group of α-aldehyde, ω-thiol PVP via reductive amination and subsequently conjugating tyrocidine to the ω-thiol end-group via an acid labile β-thiopropionate linkage (Scheme 1 (C)). The resultant constructs are self-assembled into micellar structures, with the hydrophobic peptide forming the core, and PVP forming the corona, decorated with targeting ligands.

In the first step, the peptide ligand GSRSKGT (Figure S5) was conjugated to ~2% of the heterotelechelic PVP_{4K} and PVP_{9K} α-chain ends, through the glycine residue at the *N*-termini, by reductive amination. GSRSKGT is a hydrophilic peptide, selected from a list of targeting peptide sequences, screened by Eda *et al*.[45] and found to selectively bind to the surfaces of erythrocytes infected with *P. falciparum.* Several other ligands, reported by the Eda *et al*., more specifically target *P. falciparum* infected erythrocytes, however, due to their hydrophobic properties, we anticipated that this would either interfere with the self-assembly process or diminish their expression on nanoparticle surfaces. Consequently, we chose the hydrophilic GSRSKGT peptide. Elias *et al*.[46] reported that low targeting ligand density on micelle surfaces is ideal for proper orientation with cognate receptors and effective target binding, therefore the conjugates were only sparsely decorated with the targeting ligand. Selective conjugation with the glycine residue on the N-terminus of GSRSKGT was achieved by conducting the experiment at a pH two units lower than the pK_a of the peptide ligand's ω-amino acid.[44]

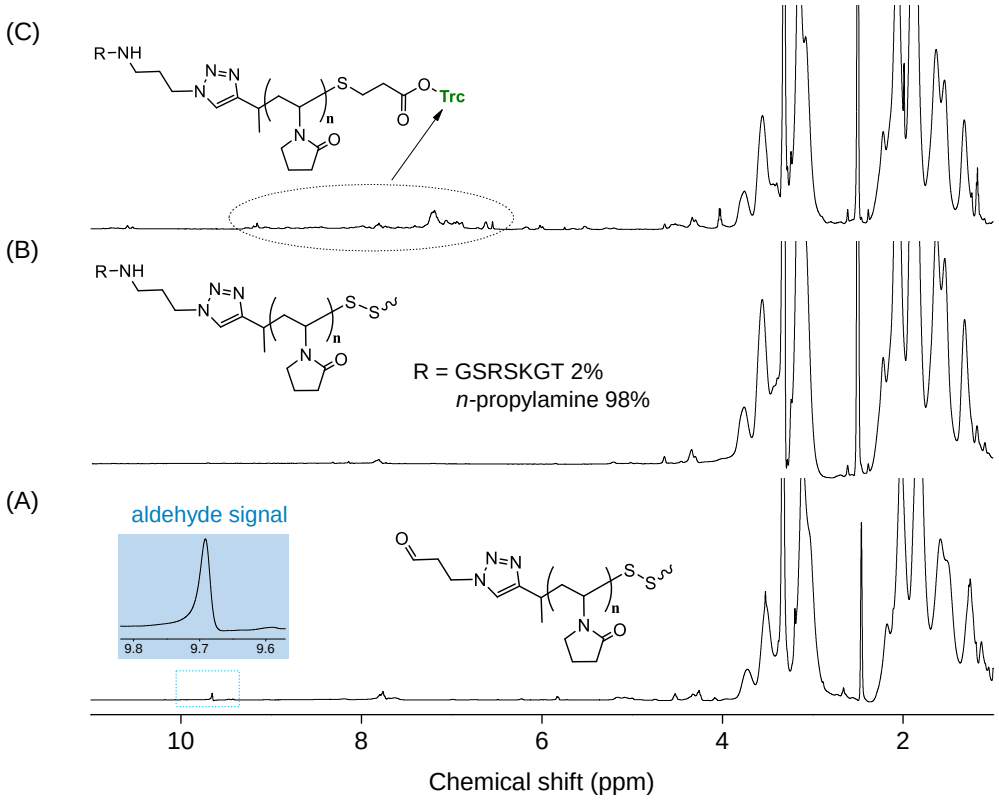

Figure 1. ^{1}H NMR spectra of (A) α-aldehyde, ω-thiol/disulfide PVP_{4K}, (B) α-GSRSKGT, ω-thiol/disulfide PVP_{4K} and (C) α-GSRSKGT, ω-tyrocidine PVP_{4K} bioconjugates.

The rest of the α-aldehyde end-groups were passivated with *n*-propylamine, also under reductive amination conditions to prevent deleterious side reactions with amine functionalities of Trc, or on other biomolecules in subsequent assays. ^{1}H NMR analysis of the α-end-modified PVP showed complete disappearance of the aldehyde signal at 9.7 ppm (Figure 1 (B)), presumably due to successful chain-end modification. It is not possible, however, to unequivocally assign the ligand peaks because of the very small extent of ligand functionalization, and spectral overlap of ligand signals with PVP backbone signals. A qualitative ninhydrin Kaiser test[47](Figure S7) was performed after purification of the α-end-modified PVP via dialysis and the presence of the peptide ligand on the polymer chain end is considered the only possible explanation of the positive Kaiser test. Similarly, we modified the α-aldehyde group of PVP_{4K} and PVP_{9K} with 100% of *n*-propylamine to design controls against which the targeting efficiency of the GSRSKGT ligand functionalized constructs would be

evaluated. PVP_{4K} was also modified with 1% aminofluorescein via reductive amination to facilitate confocal fluorescence microscopy imaging of the PVP-Trc conjugate treated cells.

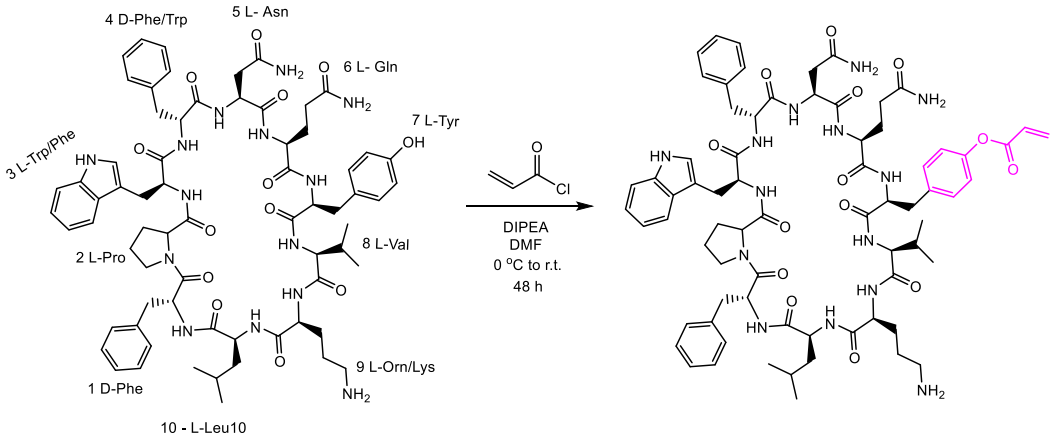

Scheme 2. Synthesis of a tyrocidine based Michael acceptor (Trc acrylate) by targeting acrylate modification of the tyrosine position 7 on the Trc decapeptide structure.

The second step towards polymer-peptide conjugate synthesis was to couple the antimicrobial Trc cyclic peptides to α-GSRSKGT, ω-thiol PVP via Michael addition. To facilitate thiol-ene coupling, a Trc based Michael acceptor was synthesized by introducing an acrylate functionality on the decapeptide structure. The tyrosine residue (residue 7) of the Trc, bearing a hydroxyl group was modified with acryloyl chloride, in presence of the excess DIPEA as organic base (Scheme 2). The base has the role of deprotonating the hydroxyl moiety, making it a good nucleophile and enabling its selective nucleophilic substitution with acryloyl chloride. Successful modification was confirmed by UPLC-MS spectrometry. The elution profiles of modified Trc (Figure 2 (A)) show a shift towards higher retention times, due to an expected increase in hydrophobicity coupled with decreased polarity following the acrylation, which causes an increased interaction with the C_{18} stationary phase. Furthermore, the molecular ion mass peaks for Trc acrylate analogues (C, B and A) differ from the 'native' Trc analogues by 54.02, corresponding to the addition of one acrylate moiety per Trc molecule (Figure 2(B)). The peaks at 11.62, 12.64 and 14.23 minutes are attributed to modified tryptocidines, functionalised on either L-Lys or L-Orn positions to form acrylamide.

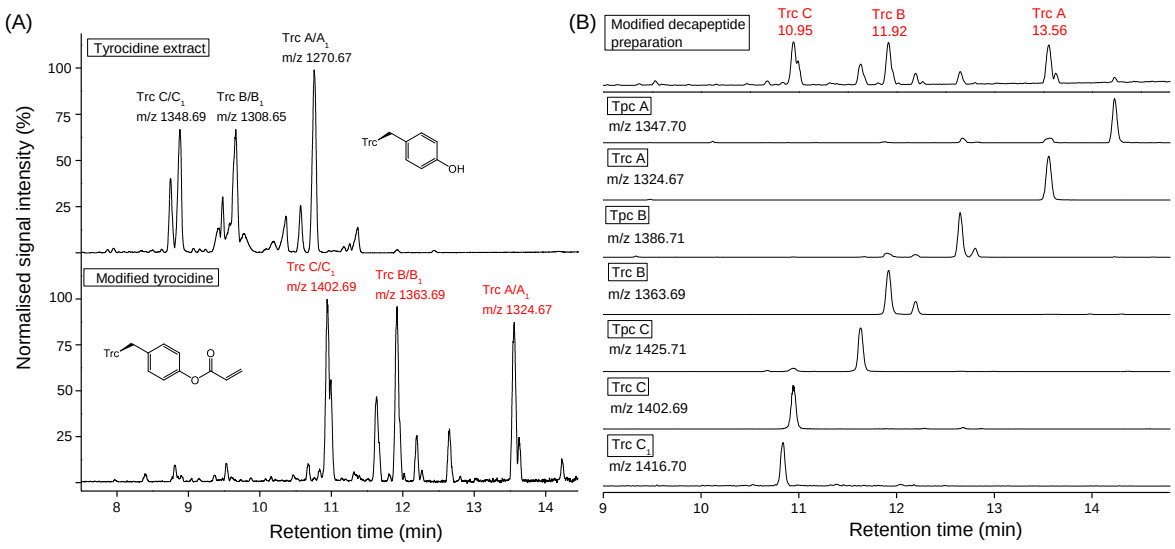

Figure 2. (A) UPLC-MS elution profiles of tyrocidine (top) and tyrocidine acrylate (bottom) and (B) the extracted ion chromatograms from the UPLC-MS analysis is of four modified Trc acrylates (Trc A, B, C and C1) and three modified Tpc acrylates (TpcA, B and C).

The final step was to conjugate the Trc acrylate to the α-GSRSKGT, ω-thiol PVP via a thiol-ene Michael addition click reaction, linking Trc to PVP via a β-thiopropionate bond. In order to maximize the thiol end-functionalities, sodium borohydride was used to reduce the disulfide-bridge linked heterotelechelic PVP chains whilst DIPEA catalysed the Michael addition.[48,49] The reaction proceeded for 48 h in DMF and the conjugate was purified by dialysis, first against water/ethanol (1:1, v/v) to remove unconjugated peptide, and then against water for an additional 24 h and lyophilized. ^{1}H NMR analysis (Figure 1 (C)), revealed the appearance of signals attributable to Trc's aromatic amino acid residues. To provide further proof of conjugation, diffusion ordered NMR spectroscopy (DOSY) was carried out to separate the NMR peaks according to the individual chemical components in solution. The solution components were found to have the same diffusion coefficient (Figure S11).

Self-assembly of the PVP-Trc conjugate. The self-assembly of linear amphiphilic diblock copolymers, induced by selective solvation in aqueous solutions, is a well-established field of study.[50] Structural parameters including overall degree of polymerization, block ratios and architecture, as well as experimental parameters such as temperature, pH and concentration

can be used to tune aggregate morphology.[51] Typically, the amphiphilic block copolymer is dissolved in a common solvent, before adding water to induce the aggregation of the hydrophobic block segment (Scheme 3), and water addition is continued to transform morphology[52] and/or stabilize the formed aggregate.[50] The self-assembly of non-linear hybrid materials such as cyclic-peptides-*block*-linear polymers is also particularly interesting due to potential applications in therapeutics [33] and separation technologies.[53] Significant strides are being made in understanding the parameters which govern the self-assembly of cyclic peptides-*block*-linear polymers, including the cyclic peptide's amino acid sequence, the linear polymer's chain length, the number of linear polymers tethered to the peptide, concentration and additives.[53]

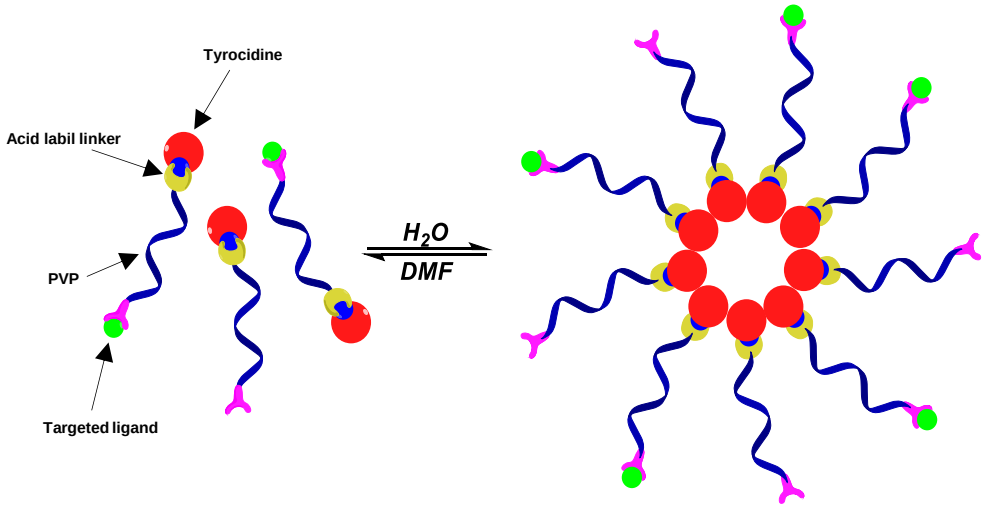

Scheme 3. Schematic representation of the PVP-Trc conjugates self-assembly process.

With the goal of preparing spherical micelles by self-assembling the PVP-Trc conjugates (Scheme 3), we prepared aggregate solutions of our conjugates by slowly adding water to DMF (common solvent) solutions of the conjugates until water was in excess to DMF. This was done to kinetically stabilize the formed aggregates before completely removing the DMF by dialysing against water with 10 000 MWCO dialysis tubing. The resultant conjugates were characterized by TEM and DLS as depicted in Figure 3.

TEM analysis revealed the formation of spherical aggregates for conjugates formed with both PVP_{4K} and PVP_{9K} (Figure 3 (A) and (C)). The average sizes of the spheres derived from TEM images were 206 nm and 124 nm for PVP_{4K}-Trc and PVP_{9K}-Trc, respectively (Figure 3 (B) and (D)). DLS characterization revealed aggregate average sizes of 356 nm and 266 nm for PVP_{4K}-Trc and PVP_{9K}-Trc, respectively (Figure 3 (E)), which highlighted that the self-assembled aggregates derived from higher M_n = 9300 g·mol^{-1} were smaller than the ones derived from the lower M_n = 4000 g·mol^{-1}, supporting the observations from TEM analysis. A similar observation was made by Lonsdale and Monteiro, who prepared so-called tadpole-shaped cyclic polystyrene-block-polyacrylic acid copolymers,[54] and Tang *et al*.[55] who analysed micelle-forming ABC triblock copolymers. The critical micelle concentration (CMC) of the PVP-Trc conjugates was determined by fluorimetry using a pyrene probe[56] (Figure 3 (F)). It is known that the lower the CMC value, the more thermodynamically stable the constructs. The CMCs of PVP_{4K}-Trc and PVP_{9K}-Trc conjugates were found to be 5.0×10^{-2} mM and 3.5×10^{-2} mM, respectively, corroborating the TEM and DLS findings by infering greater thermodynamic stability for the higher molecular weight conjugates.

Aggregate morphologies formed by self-assembly of linear block copolymers can be thermodynamically controlled by varying block ratios. Long hydrophilic to hydrophobic block ratios produce spherical micelles, shorter hydrophilic to hydrophobic ratios produce lamellar morphologies and cylindrical aggregates are produced in a narrow window of block ratios.[57] The aggregate morphologies observed herein suggest that the self-assembly process observed the same precepts controlled by the ratios of hydrophilic to hydrophobic blocks. It is reasonable to assume the observed morphologies are close to equilibrium structures since water was added very slowly to DMF solutions of the polymer-peptide conjugates.

Earlier in the study, we described the synthesis of α-aldehyde, ω-thiol, heterotelechelic PVP, which was subsequently modified by incorporating a GSRSKGT targeting ligand on the α end-chain and tyrocidine on the ω end-chain, to yield PVP-Trc bioconjugates capable of self-assembly into spherical aggregates. In our previous work, model compounds were employed to modify heterotelechelic PVP end-groups, to yield a model drug delivery construct. The release capacity of the model drug construct was evaluated by cleaving the β-thiopropionate ester linkage under mild acidic conditions.[34] We followed up on the findings of the model study by evaluating the ease of release of tyrocidine from the PVP-Trc conjugates. The potential activity and selectivity of the bioconjugates were evaluated against asexual *P. falciparum* infected erythrocytes, by determining the IC_{50} and HC_{50}.

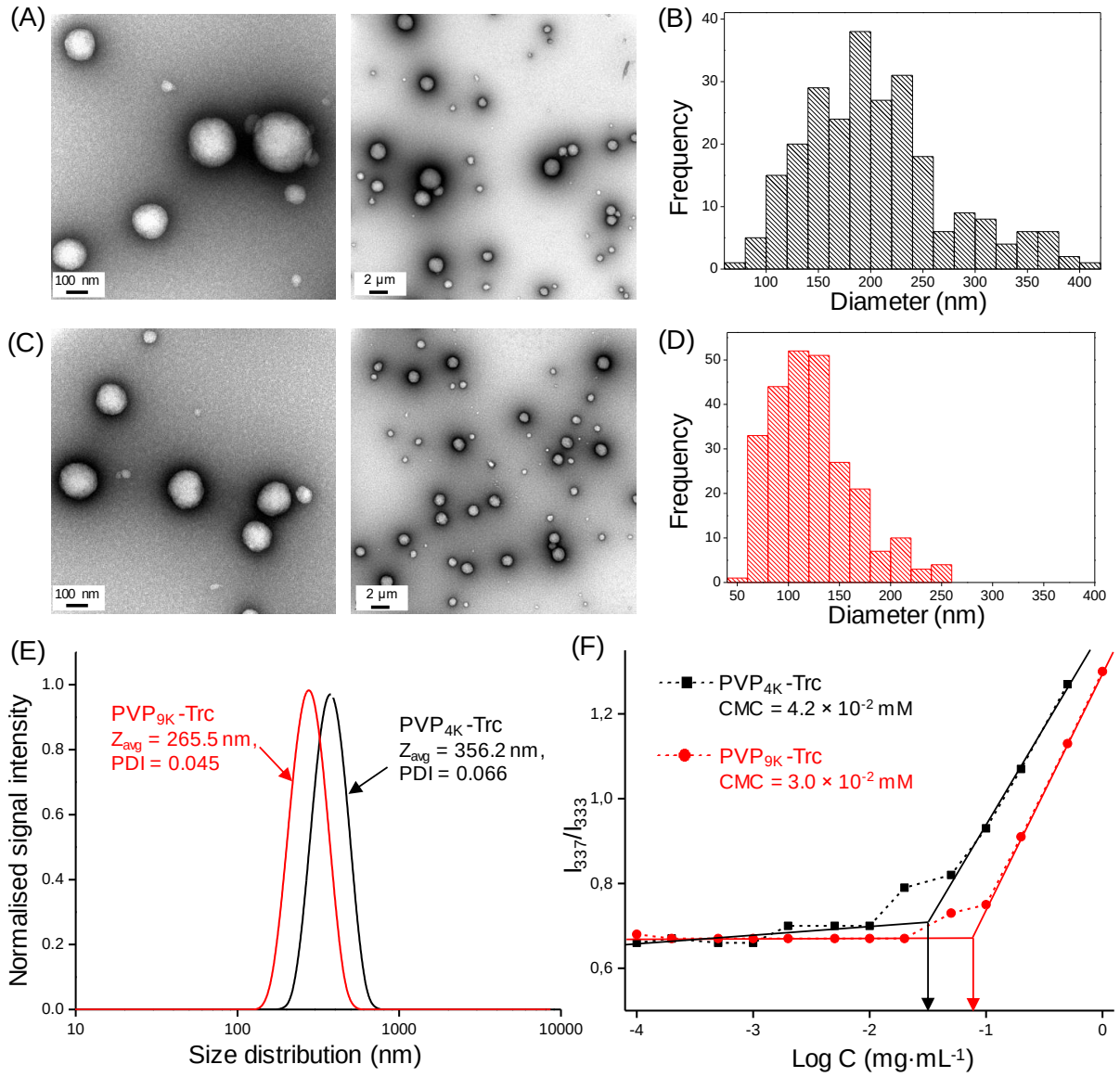

Figure 3. TEM images and DLS analysis corresponding to the aggregates formed from PVP_{4K}-Trc conjugate (Images A and histogram B) and PVP_{9K}-Trc conjugate (Images C and histogram D). The size distribution profiles for both PVP-tyrocidine conjugates are shown in (E). CMC determination by fluorescence intensity (pyrene) for PVP_{4K}-Trc and PVP_{9K}-Trc conjugates is shown in (F).

Tyrocidine release studies. A qualitative study was performed on the release of tyrocidines over time as monitored by UPLC-MS (Figure 4). PVP_{3K}, M_n = 2700 g·mol^{-1}, was conjugated to tyrocidine using methods earlier described to yield conjugate **5**. Low molecular weight PVP was employed to facilitate ionisation under normal MS conditions. A freeze-dried sample of the conjugate was dissolved in a phosphate buffer (pH = 5.5). Samples were taken at the onset of the study and after 14 h, immediately frozen in liquid nitrogen and stored until analysis. The average molar mass of the conjugate is approximately 4000 g·mol^{-1}, hence, the penta-charged molecular ion (733.97 Da) was chosen to represent the conjugate, while TrcA was selected for monitoring the released tyrocidines. It is important to highlight that the chromatogram shown at 0 h is not an absolute control because of the time taken for the sample to thaw prior to injection. Consequently, released tyrocidines are seen in the chromatogram (Figure 4(A)). However, from the onset, t = 0, to the end of the experiment, t = 14 h, the count of the released tyrocidines (TrcA) increased substantially from 140 to 844 (Figure 4(C) and 4(F)).

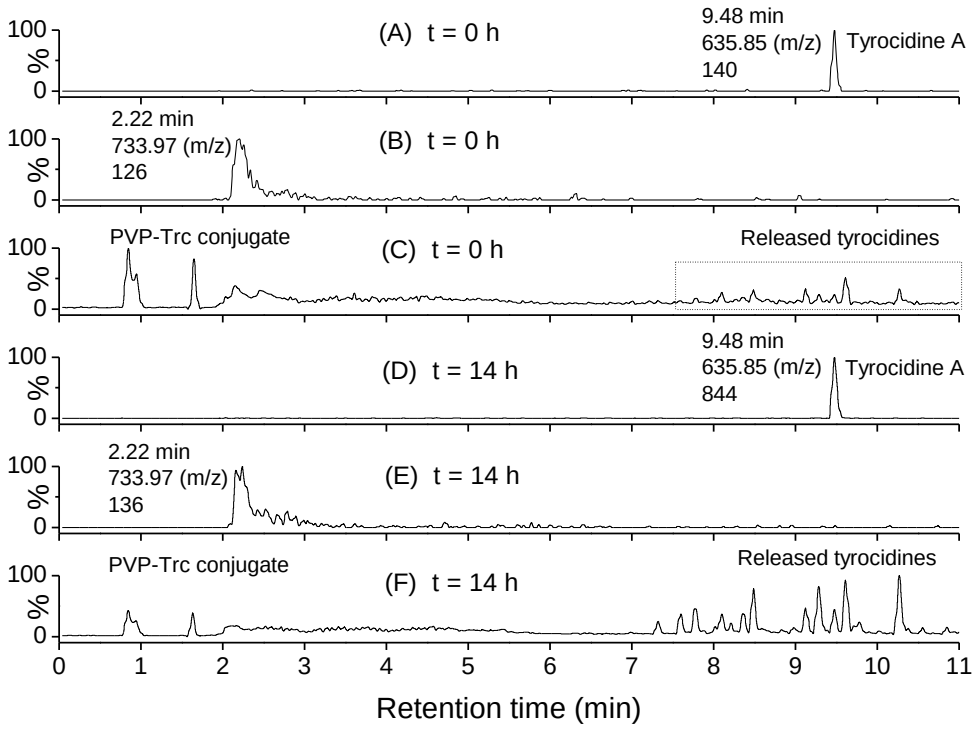

Figure 4. UPLC-MS chromatograms of the release of tyrocidine from PVP-Trc conjugate 5 over 14 h at pH = 5.5. The penta-charged molecular ion at *m/z* 733.97 represents the conjugate. TrcA represents the released tyrocidines. (A) and (D) represent the extracted ion chromatograms of Trc A at 0 h and 14 h. (B) and (E) represent extracted ion chromatograms of the PVP-Trc conjugate pentavalent ion (733.97) at 0 h and 14 h respectively. (C) and (F) represent the UPLC chromatograms for conjugate 5 after 0 h and 14 h respectively.

The breakdown of the individual tyrothricin components released is given in Figure 5. Each peak is labelled with its retention time, major *m/z* detected (doubly charged) and molecular count. Two important observations are derived from the deconvoluted chromatograms. First, the chromatograms show that all three major tyrocidine species are released without any alterations to the original structural state. This is important because some studies have reported diminished biological activity as consequence of structural modification of drugs, which inevitably interferes with mechanisms of action and uptake.[58] Second, the three main tryptocidine species were also released. This was not anticipated as tryptocidines are conjugated through L-Orn or L-Lys residues which results in amide formation. However, the β-thio moiety appears to have destabilised both the ester and amide linkages under acidic conditions.

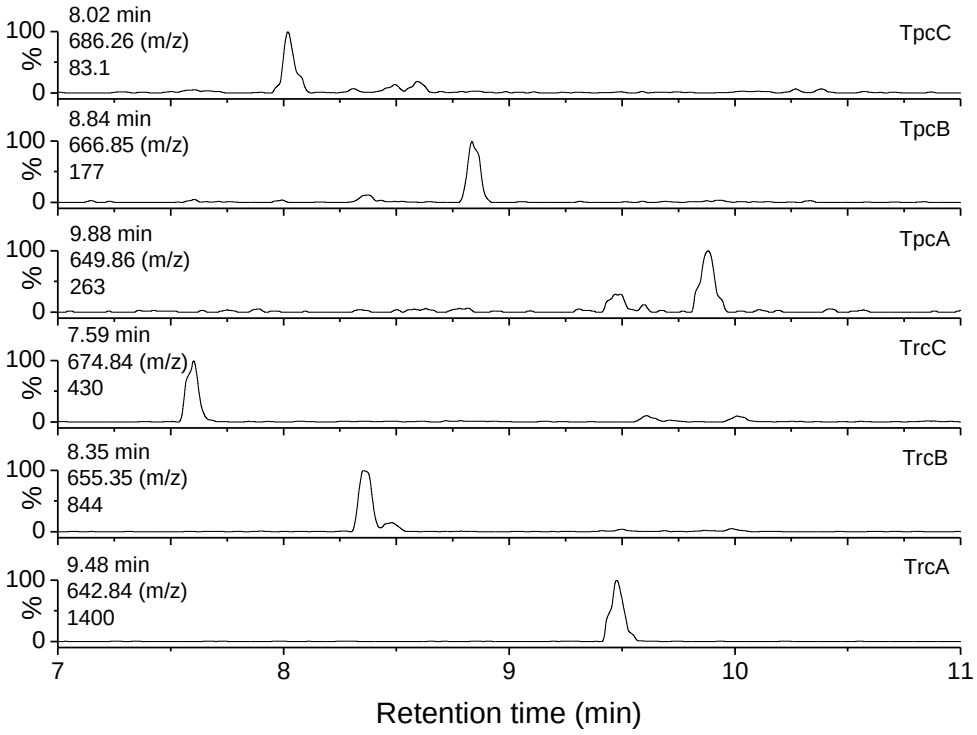

Figure 5. Extracted ion chromatograms from the UPLC-MS analysis of the individual components of released tyrocidines and tryptocidines. The chromatograms are labelled on the left side with retention time of detected peptide ion (min, top value), *m/z* detected for doubly charged molecular ion (middle value) and ion count (bottom value).

***In vitro* activity of the PVP-Trc conjugates towards the asexual erythrocytic stages of *P. falciparum*.** Our hypothesis for the inhibition of asexual erythrocytic parasites is based on potential uptake of the conjugates and subsequent targeted release of Trc from PVP in the infected cells due to low pH in the parasite's food vacuole. Alternatively, the Trcs can be released just outside the cells due to localised lower pH, because of the anaerobic production of high levels of lactate/lactic acid by the growing malaria parasite.[59, 60] Localised release would be highly beneficial as the tyrocidines then pass over the membrane due to their amphipathic character[61, 62] and exert their activity on the parasite targets. The goal was therefore to determine the *in vitro* anti-plasmodial activity of the conjugates in comparison with free Trc. For this comparison we utilised the IC_{50} and selectivity towards infected erythrocytes based on the HC_{50}. The IC_{50} values of the conjugates were determined using the SYBR Green I based assay on NF54 strain of *P. falciparum* parasites. Dose-response curves are shown in

Figure 6 whilst Table 2 summarises the data in the form of IC_{50} and HC_{50} concentrations, and selectivity index (SI) for the various conjugates towards infected erythrocytes. According to the IC_{50} parameter there was approximately a 35-fold loss in activity for the PVP-Trc conjugates relative to the free Trc preparation (Table 2 and Figure 6(A)), indicating that the Trc is not taken up as effectively into the parasite when ligated to PVP. The activity loss could be because of the particle size hindering uptake, although localised release is still possible. However, regardless of how the Trcs reach their target, the general activity PVP-Trc remained in the $ng \cdot mL^{-1}$ range, inferring good *in vitro* activity against *P. falciparum* infected erythrocytes. However, the haemolytic activity of the PVP-Trc conjugate was significantly lower compared to unconjugated Trc preparation (Figure 6(B)). There was no significant difference in activity between the two conjugate groups differing in size, *i.e.* in the case of both non-targeted (**1, 2**) and targeted (**3, 4**) conjugates (Figure 6(A)). However, the antimalarial activity of the conjugates with similar size differed significantly with respect to the presence of the targeting ligand (Figure 6(A)). These observations suggest that PVP-tyrocidine conjugates decorated with the targeting moiety target the infected erythrocytes more efficiently in comparison to the conjugates without the targeting ligand.

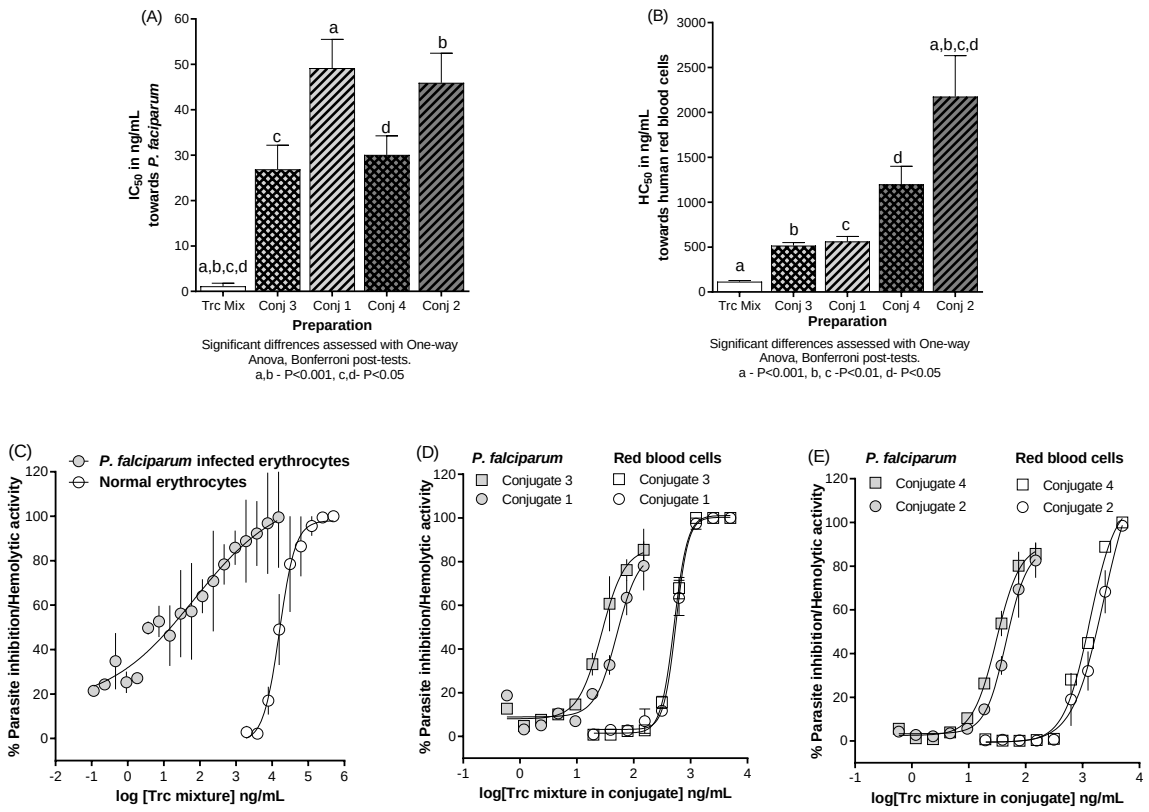

Figure 6. Dose-response evaluation of Trc and PVP-Trc conjugates against *P. falciparum* parasites and human erythrocytes. Activity and haemolytic toxicity of non-targeted (1, 2) and targeted (3, 4) PVP-Trc conjugates. (A) Comparative histogram of the IC_{50} activity parameters for free Trc and PVP-Trc conjugates towards *P. falciparum* infected erythrocytes. (B) Comparative histogram of the HC_{50} haemolytic parameter for Trc and PVP-Trc conjugates towards normal erythrocytes. Dose-response of (C) free Trc, (D) PVP_{4K}-Trc and (E) PVP_{9K}-Trc conjugates towards *P. falciparum* infected erythrocytes (grey symbols) and normal erythrocytes (clear symbols). For all graphs, data are the mean of three independent determinations with standard error of the mean.

Haemolytic toxicity determination. To ensure that the *in vitro* activity observed for the PVP-Trc conjugates was not just due to haemolysis induced by the Trc, the *in vitro* haemolytic activity of the PVP-Trc conjugates was determined on human erythrocytes compared to that of Trc alone. Haemoglobin is released from erythrocytes with a compromised membrane integrity, by measuring its absorbance, the fraction of erythrocytes that no longer have an intact membrane, *i.e.* non-viable erythrocytes, is directly determined.[15, 63] The concentrations leading to 50% haemolysis (HC_{50}) for the conjugates **1-4** are summarised in Table 2 and Figure 6(E).

Table 2. Summary of activity and toxicity parameters (IC_{50}, HC_{50} and SI) of Trc and its conjugates with PVP with erythrocytic stage of *P. falciparum* as target

Sample	Activity against *P. falciparum* infected RBC in ng/mL (nM)	Haemolytic Toxicity towards human erythrocytes in ng/mL (nM)	Selectivity Index (SI)
	IC_{50} ± SEM*	HC_{50} ± SEM*	HC_{50} /IC_{50}
Tyrocidine mixture	1.1 ± 0.7 (0.83)	115 ± 13 (87)	105
Conjugate 1[a]	49 ± 6.3 (37)	563 ± 57 (425)	11
Conjugate 3[b]	27 ± 5.3 (20)	516 ± 34 (389)	19
Conjugate 2[c]	46 ± 6.5 (35)	2176 ± 457 (1641)	46
Conjugate 4[d]	30 ± 4.2 (23)	1200 ± 200 (905)	40

*Data are means of three independent biological replicates ± SEM for the proliferative and haemolysis assays. [a]α-propyl-PVP_{4K}-Trc, nM concetrations were calculated from the average M_r of 1325.8 of the Trc preparation (refer to Table S3) [b] α-$GSRSKGT_{(2\%)}$, $propyl_{(98\%)}$-PVP_{4K}-Trc, [c]α-propyl-PVP_{4K}-Trc, [d]α-$GSRSKGT_{(2\%)}$, $propyl_{(98\%)}$-PVP_{9K}-Trc.

All the tested preparations show appreciable selectivity towards the parasitized erythrocyte, with the free Trc preparations having the apparent highest selectivity at 105. This selectivity of Trcs correlates with previous reports.[16, 36] However, it is important to highlight that SI only considers a narrow concentration and activity response, which can be misleading, specifically if the free Trc SI of 105 is taken as is. One must consider the entire dose response from which we observed that the free Trc complex appears to lose some of its selectivity at >1.1 $mg \cdot mL^{-1}$ and shows almost no selectivity at >80% of the activity response. All of the Trc-PVP the conjugates were observed to be selective over the whole concentration range (compare dose response graphs in Figure 6(C-E)).

PVP-Trc conjugates showed 4- to 19-fold lower haemolytic activity towards erythrocytes relative to free Trc which is a significant reduction in toxicity (refer to Figure 6(B) for statistical details). This suggests that conjugation of tyrocidine to PVP and the subsequent self-assembly decreases the inherent haemolytic activity of the Trc preparation. Furthermore, the size differences between the conjugates derived from low molecular weight PVP_{4K} (**1, 3**)

and high molecular weight PVP_{9K} (**2, 4**) appear to play a role in influencing the haemolytic toxicity (Figure 6(B) and Table 2). Therefore, increasing the molar mass of PVP (approximately 2-fold) seems to lower haemolytic toxicity even further, which could indicate effective shielding of the toxic peptide in the conjugate particle. This suggests different sized nanomaterials cannot only be viewed as therapeutic carriers but can also play crucial roles in mediating biological function and toxicity.[64]

The influence of the targeting ligand on haemolytic activity seems to be dependent on conjugate size, for the conjugates with lower M_n, the ligand appears to have an insignificant influence, whilst a significant difference ($P<0.05$) is observed for the higher M_n. It could be hypothesised that the smaller particle size of the higher M_n conjugates allows more ligand-membrane interactions per particle and this then benefits of polymer-peptide conjugation recognition and selectivity for infected cells.

From a drug safety point of view, it is important to note that for all conjugates, their IC_{50} values were significantly below their HC_{50} values, signifying that the conjugates target infected erythrocytes before lysing healthy erythrocytes as substantiated by selectivity indices (SI) above 10 (Table 2).[36] Although the conjugates are 11-47 fold more selective towards infected erythrocytes than healthy erythrocytes, this selectivity remains over the whole concentration range, which is not the case for the free Trc (refer to Figure 6 and discussion above). Crucially, all conjugates showed significantly ($P<0.05$, n=3) lower cytoxicity (cell viability $\geq$ 95%), relative to free Trc (cell viability $\geq$ 62%) against HepG2 cells at 10 μg/mL (Table S5 and Figure S12).

Cell imaging of PVP-Trc conjugate-treated *P. falciparum* cultures. Light microscopy and confocal fluorescence microscopy CFM were employed to evaluate the effect of PVP-Trc conjugates on *P. falciparum* infected erythrocytes. Smears of the conjugate-treated

parasite cultures and growth control were taken at 24 h and subsequently stained with Giemsa, which stains the malaria parasite purple when viewed under the light microscope. The growth control with healthy parasites after 24 h is shown in Figure 7 (A) while PVP-Trc conjugate-treated *P. falciparum* infected erythrocytes (Figure 7 (B) shows complete elimination of the parasite, post treatment. Similarly, smears of the PVP-Trc conjugate-treated parasite cultures and growth controls were taken at 48 h and prepared for CFM analysis. Conjugate **3** was tagged with 1% of fluorescein to visualise the distribution of the nanoparticles between normal erythrocytes and parasite infected ones. The growth control image (Figure 7(C)) shows some autofluorescence, however, the fluorescence intensity increases significantly post-treatment (Figure 7(D)). The intense fluorescence which is visible on the circumference of the cells can be explained by referring to the activity results (Figures 6(A) and (B)).

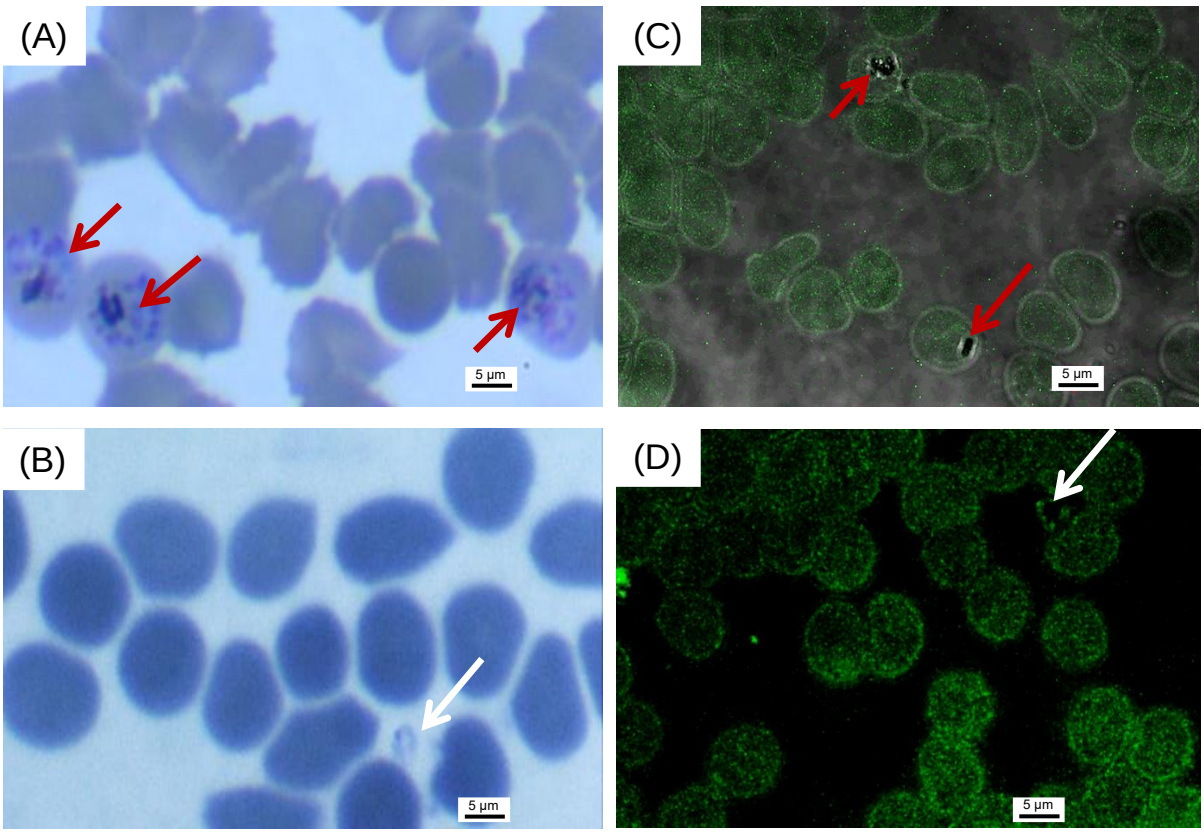

Figure 7. Giemsa-stained (A, B) and CFM (C, D) blood smear images from *P. falciparum* cultures treated with PVP-Trc conjugate (for 24 h). (A) and (C) are growth controls with red arrows showing the parasites in cells. (B) and (D) are post-treatment images with white arrows showing dead parasite outside of cells.

The incorporation of the targeting ligand likely leads to enhanced accumulation on or in the *P. falciparum* infected erythrocytes. However, despite the differing fluorescence intensity on the cells, Figure 7(D) shows that the nanoparticles are present in and around both infected and normal erythrocytes. This could be a consequence of the parasite protein that is shed during the invasion process,[65-68] which associates with uninfected erythrocyte membranes leading to detection by the targeting ligand. The activity results, however, show better selective activity of the ligand tagged nanoparticles, which did not translate into the haemolytic toxicity, indicating that the interaction with uninfected erythrocytes cells are non-productive.

CONCLUSIONS

The synthesis of targeted PVP-tyrocidine drug delivery constructs was facilitated by RAFT mediated polymerization which allowed for the post-polymerization incorporation of a malaria-specific targeting peptide, GSRSKGT, on the α-chain end via reductive amination. Tyrocidine, an antimicrobial peptide, was coupled on the ω-chain end via thiol-ene coupling. The resultant constructs were characterized and then self-assembled in aqueous media into micellar aggregates whose sizes had an inverse relationship with PVP chain length. We were also able to show that the peptides from the Trc preparation are released over time when exposed to acidic environments. The selective activity of the conjugates as drug delivery systems against *P. falciparum* infected erythrocytes showed that this type of conjugation of a toxic compound, in this case the Trcs, has good potential and that targeting is possible. Most notably, the targeted GSRSKGT conjugates exhibited higher selective activity relative to the non-targeted conjugates. Furthermore, the Trc conjugates derived from higher molecular weight PVP exhibited lower haemolytic toxicity relative to conjugates derived from lower molecular weight PVP. This suggests that higher molecular weights and optimised ligand density could potentially result in higher activity, lower toxicity, and consequently high selectivity indices for otherwise non-selective toxic compounds. Our conjugation approach with α-aldehyde, ω-thiol PVP and end-chain functionalization has the potential to create the so-called "silver bullet" as it allows for ligand-type targeting and programmed release of a therapeutic compound that would otherwise not be clinically viable because of toxicity and/or limited stability.

ASSOCIATED CONTENT

Supporting Information. NMR spectra, SEC chromatograms and supplementary results on tyrocidine preparation and characterizations are presented in the Supporting Information.

AUTHOR INFORMATION

Corresponding Authors

*E-mail: mra@sun.ac.za.

*E-mail: bklump@sun.ac.za

ORCID

Simbarashe Jokonya: 0000-0002-8199-3598

Marvin Langlais: 0000-0002-5315-7613

Meta Leshabane: 0000-0001-6885-1483

Paul W Reader: 0000-0002-1285-5554

Johan A Vosloo: 0000-0002-1304-6150

Dina Coertzen: 0000-0002-8408-244X

Rueben Pfukwa: 0000-0002-4816-2848

Lyn-Marie Birkholtz: 0000-0001-5888-2905

Marina Rautenbach: 0000-0001-7198-9213

Bert Klumperman: 0000-0003-1561-274X

Notes

The authors declare no competing financial interest.

ACKNOWLEDGMENTS

We acknowledge funding from the South African Research Chairs Initiative of the Department of Science and Technology (DST) and National Research Foundation (NRF) of South Africa (Grant No 46855 to BK and Grant No 84627 to LMB) and Communities of Practice in Malaria

Elimination (Grant no. 110666). We also acknowledge the central analytical facilities (CAF) staff, Marietjie Stander, Jaco Brand and Elsa Malherbe for the HPLC and NMR analyses.

REFERENCES

1. Greszta, D.; Mardare, D.; Matyjaszewski, K., " Living" radical polymerization. 1. Possibilities and limitations. *Macromolecules* **1994,** 27, (3), 638.
2. Braunecker, W. A.; Matyjaszewski, K., Controlled/living radical polymerization: Features, developments, and perspectives. *Prog. Polym. Sci.* **2007,** 32, (1), 93.
3. Druilhe, P.; Daubersies, P.; Patarapotikul, J.; Gentil, C.; Chene, L.; Chongsuphajaisiddhi, T.; Mellouk, S.; Langsley, G., A primary malarial infection is composed of a very wide range of genetically diverse but related parasites. *J. Clin. Investig.* **1998,** 101, (9), 2008-2016.
4. Snow, R. W.; Guerra, C. A.; Noor, A. M.; Myint, H. Y.; Hay, S. I., The global distribution of clinical episodes of Plasmodium falciparum malaria. *Nature* **2005,** 434, (7030), 214.
5. Bloland, P. B.; Lackritz, E. M.; Kazembe, P. N.; Were, J. B. O.; Steketee, R.; Campbell, C. C., Beyond Chloroquine: Implications of Drug Resistance for Evaluating Malaria Therapy Efficacy and Treatment Policy in Africa. *J. Infect. Dis.* **1993,** 167, (4), 932-937.
6. Gardella, F.; Assi, S.; Simon, F.; Bogreau, H.; Eggelte, T.; Ba, F.; Foumane, V.; Henry, M.-C.; Kientega, P. T.; Basco, L., Antimalarial drug use in general populations of tropical Africa. *Malar. J.* **2008,** 7, (1), 124.
7. Hoskin, D. W.; Ramamoorthy, A., Studies on anticancer activities of antimicrobial peptides. *Biochim. Biophys. Acta* **2008,** 1778, (2), 357-375.

8. Giuliani, A.; Pirri, G.; Nicoletto, S., Antimicrobial peptides: an overview of a promising class of therapeutics. *Open Life Sci.* **2007,** 2, (1), 1-33.

9. Zhang, L.-j.; Gallo, R. L., Antimicrobial peptides. *Curr. Biol.* **2016,** 26, (1), R14-R19.

10. Meng, D.-M.; Li, W.-J.; Shi, L.-Y.; Lv, Y.-J.; Sun, X.-Q.; Hu, J.-C.; Fan, Z.-C., Expression, purification and characterization of a recombinant antimicrobial peptide Hispidalin in Pichia pastoris. *Protein Expr. Purif.* **2019,** 160, 19.

11. Pouny, Y.; Rapaport, D.; Mor, A.; Nicolas, P.; Shai, Y., Interaction of antimicrobial dermaseptin and its fluorescently labeled analogs with phospholipid membranes. *Biochemistry* **1992,** 31, (49), 12416-12423.

12. Baumann, G.; Mueller, P., A molecular model of membrane excitability. *J. Supramol. Struct.* **1974,** 2, (5-6), 538-557.

13. Tang, X.-J.; Thibault, P.; Boyd, R. K., Characterisation of the tyrocidine and gramicidin fractions of the tyrothricin complex from Bacillus brevis using liquid chromatography and mass spectrometry. *Int. J. Mass Spectrom.* **1992,** 122, 153-179.

14. Hotchkiss, R. D.; Dubos, R. J., The isolation of bactericidal substances from cultures of Bacillus brevis. *J. Biol. Chem.* **1941,** 141, (1), 155-162.

15. Rautenbach, M.; Vlok, N. M.; Stander, M.; Hoppe, H. C., Inhibition of malaria parasite blood stages by tyrocidines, membrane-active cyclic peptide antibiotics from Bacillus brevis. *Biochim. Biophys. Acta* **2007,** 1768, (6), 1488-1497.

16. Leussa, A. N. N. Characterisation of small cyclic peptides

with antimalarial and antilisterial activity. Stellenbosch University, 2013.

17. Greszta, D.; Mardare, D.; Matyjaszewski, K., " Living" radical polymerization. 1. Possibilities and limitations. *Macromolecules* **1994,** 27, (3), 638-644.

18. Nordström, R.; Malmsten, M., Delivery systems for antimicrobial peptides. *Adv. Colloid Interface Sci.* **2017,** 242, 17-34.

19. Dartois, V.; Sanchez-Quesada, J.; Cabezas, E.; Chi, E.; Dubbelde, C.; Dunn, C.; Granja, J.; Gritzen, C.; Weinberger, D.; Ghadiri, M. R., Systemic antibacterial activity of novel synthetic cyclic peptides. *Am. Soc. Microbiol.* **2005,** 49, (8), 3302-3310.

20. Marr, A. K.; Gooderham, W. J.; Hancock, R. E. W., Antibacterial peptides for therapeutic use: obstacles and realistic outlook. *Curr. Opin. Pharmacol.* **2006,** 6, (5), 468-472.

21. Veronese, F. M.; Pasut, G., PEGylation, successful approach to drug delivery. *Drug. Discov. Today* **2005,** 10, (21), 1451-1458.

22. Singh, S.; Papareddy, P.; Mörgelin, M.; Schmidtchen, A.; Malmsten, M., Effects of PEGylation on membrane and lipopolysaccharide interactions of host defense peptides. *Biomacromolecules* **2014,** 15, (4), 1337-1345.

23. Veronese, F. M.; Pasut, G., PEGylation, successful approach to drug delivery. *Drug. Discov. Today* **2005,** 10, (21), 1451.

24. Atassi, M. Z.; Manshouri, T., Synthesis of tolerogenic monomethoxypolyethylene glycol and polyvinyl alcohol conjugates of peptides. *J. Protein Chem.* **1991,** 10, (6), 623-627.

25. Melo, M. N.; Ferre, R.; Castanho, M. A. R. B., Antimicrobial peptides: linking partition, activity and high membrane-bound concentrations. *Nat. Rev. Microbiol.* **2009,** 7, (3), 245-250.

26. Gauthier, M. A.; Klok, H.-A., Peptide/protein–polymer conjugates: synthetic strategies and design concepts. *ChemComm* **2008**, (23), 2591-2611.

27. Sun, H.; Hong, Y.; Xi, Y.; Zou, Y.; Gao, J.; Du, J., Synthesis, Self-Assembly, and Biomedical Applications of Antimicrobial Peptide–Polymer Conjugates. *Biomacromolecules* **2018,** 19, (6), 1701-1720.

28. Boyer, C.; Liu, J.; Bulmus, V.; Davis, T. P.; Barner-Kowollik, C.; Stenzel, M. H., Direct Synthesis of Well-Defined Heterotelechelic Polymers for Bioconjugations. *Macromolecules* **2008,** 41, (15), 5641-5650.

29. Huin, C.; Eskandani, Z.; Badi, N.; Farcas, A.; Bennevault-Celton, V.; Guégan, P., Anionic ring-opening polymerization of ethylene oxide in DMF with cyclodextrin derivatives as new initiators. *Carbohydr. Polym.* **2013,** 94, (1), 323-331.

30. Grover, G. N.; Maynard, H. D., Protein–polymer conjugates: synthetic approaches by controlled radical polymerizations and interesting applications. *Curr. Opin. Chem. Biol* **2010,** 14, (6), 818.

31. Zhao, W.; Liu, F.; Chen, Y.; Bai, J.; Gao, W., Synthesis of well-defined protein–polymer conjugates for biomedicine. *Polymer* **2015,** 66, A1-A10.

32. Liu, R.; Zhang, Y.; Zhao, X.; Agarwal, A.; Mueller, L. J.; Feng, P., pH-Responsive Nanogated Ensemble Based on Gold-Capped Mesoporous Silica through an Acid-Labile Acetal Linker. *J. Am. Chem. Soc.* **2010,** 132, (5), 1500.

33. Larnaudie, S. C.; Sanchis, J.; Nguyen, T.-H.; Peltier, R.; Catrouillet, S.; Brendel, J. C.; Porter, C. J. H.; Jolliffe, K. A.; Perrier, S., Cyclic peptide-poly(HPMA) nanotubes as drug delivery vectors: In vitro assessment, pharmacokinetics and biodistribution. *Biomaterials* **2018,** 178, 570-582.

34. Nash, M. A.; Waitumbi, J. N.; Hoffman, A. S.; Yager, P.; Stayton, P. S., Multiplexed Enrichment and Detection of Malarial Biomarkers Using a Stimuli-Responsive Iron Oxide and Gold Nanoparticle Reagent System. *ACS Nano* **2012,** 6, (8), 6776-6785.

35. Verlinden, B. K.; Niemand, J.; Snyman, J.; Sharma, S. K.; Beattie, R. J.; Woster, P. M.; Birkholtz, L.-M., Discovery of Novel Alkylated (bis)Urea and (bis)Thiourea Polyamine Analogues with Potent Antimalarial Activities. *J. Med. Chem.* **2011,** 54, (19), 6624-6633.

36. Kim, S.-Y.; Heo, M. B.; Hwang, G.-S.; Jung, Y.; Choi, D. Y.; Park, Y.-M.; Lim, Y. T., Multivalent Polymer Nanocomplex Targeting Endosomal Receptor of Immune Cells for Enhanced Antitumor and Systemic Memory Response. *Angewandte Chemie International Edition* **2015,** 54, (28), 8139-8143.

37. Rossy, J.; Williamson, D. J.; Benzing, C.; Gaus, K., The integration of signaling and the spatial organization of the T cell synapse. *Frontiers in Immunology* **2012,** 3, 352.

38. Boyer, C.; Liu, J.; Bulmus, V.; Davis, T. P., RAFT polymer end-group modification and chain coupling/conjugation via disulfide bonds. *Aust. J. Chem.* **2009,** 62, (8), 830-847.

39. Guinaudeau, A.; Mazières, S.; Wilson, D. J.; Destarac, M., Aqueous RAFT/MADIX polymerisation of N-vinyl pyrrolidone at ambient temperature. *Polym. Chem* **2012,** 3, (1), 81-84.

40. Pound, G.; Eksteen, Z.; Pfukwa, R.; McKenzie, J. M.; Lange, R. F. M.; Klumperman, B., Unexpected reactions associated with the xanthate-mediated polymerization of N-vinylpyrrolidone. *J. Polym. Sci. A Polym. Chem.* **2008,** 46, (19), 6575-6593.

41. Langlais, M.; Coutelier, O.; Destarac, M., Thiolactone-Functional Reversible Deactivation Radical Polymerization Agents for Advanced Macromolecular Engineering. *Macromolecules* **2018,** 51, (11), 4315-4324.

42. Matyjaszewski, K., Macromolecular engineering: From rational design through precise macromolecular synthesis and processing to targeted macroscopic material properties. *Prog. Polym. Sci.* **2005,** 30, (8), 858.

43. Guinaudeau, A.; Mazières, S.; Wilson, D. J.; Destarac, M., Aqueous RAFT/MADIX polymerisation of N-vinyl pyrrolidone at ambient temperature. *Polym. Chem.* **2012,** 3, (1), 81-84.

44. Reader, P. W.; Pfukwa, R.; Jokonya, S.; Arnott, G. E.; Klumperman, B., Synthesis of α,ω-heterotelechelic PVP for bioconjugation, via a one-pot orthogonal end-group modification procedure. *Polym. Chem.* **2016,** 7, 6450.

45. Eda, K.; Eda, S.; Sherman, I. W., Identification of peptides targeting the surface of Plasmodium falciparum-infected erythrocytes using a phage display peptide library. *Am. J. Trop. Med. Hyg.* **2004,** 71, (2), 190-195.

46. Elias, D. R.; Poloukhtine, A.; Popik, V.; Tsourkas, A., Effect of ligand density, receptor density, and nanoparticle size on cell targeting. *Nanomedicine* **2013,** 9, (2), 194.

47. Kaiser, E.; Colescott, R. L.; Bossinger, C. D.; Cook, P. I., Color test for detection of free terminal amino groups in the solid-phase synthesis of peptides. *Anal. Biochem.* **1970,** 34, (2), 595.

48. Chan, J. W.; Hoyle, C. E.; Lowe, A. B.; Bowman, M., Nucleophile-initiated thiol-michael reactions: effect of organocatalyst, thiol, and ene. *Macromolecules* **2010,** 43, (15), 6381-6388.

49. Li, G.-Z.; Randev, R. K.; Soeriyadi, A. H.; Rees, G.; Boyer, C.; Tong, Z.; Davis, T. P.; Becer, C. R.; Haddleton, D. M., Investigation into thiol-(meth) acrylate Michael addition reactions using amine and phosphine catalysts. *Polym. Chem.* **2010,** 1, (8), 1196-1204.

50. Mai, Y.; Eisenberg, A., Self-assembly of block copolymers. *Chem. Soc. Rev.* **2012,** 41, (18), 5969.

51. Rodríguez-Hernández, J.; Chécot, F.; Gnanou, Y.; Lecommandoux, S., Toward 'smart' nano-objects by self-assembly of block copolymers in solution. *Prog. Polym. Sci.* **2005,** 30, (7), 691-724.

52. Shen, H.; Eisenberg, A., Morphological Phase Diagram for a Ternary System of Block Copolymer PS310-b-PAA52/Dioxane/H2O. *J. Phys. Chem. B* **1999,** 103, (44), 9473-9487.

53. Shu, J. Y.; Panganiban, B.; Xu, T., Peptide-polymer conjugates: from fundamental science to application. *Annu. Rev. Phys. Chem.* **2013,** 64, 631-657.

54. Lonsdale, D. E.; Monteiro, M. J., Synthesis and self-assembly of amphiphilic macrocyclic block copolymer topologies. *J. Polym. Sci. A* **2011,** 49, (21), 4603-4612.

55. Tang, Y.; Liu, S. Y.; Armes, S. P.; Billingham, N. C., Solubilization and controlled release of a hydrophobic drug using novel micelle-forming ABC triblock copolymers. *Biomacromolecules* **2003,** 4, (6), 1636-1645.

56. Ray, G. B.; Chakraborty, I.; Moulik, S. P., Pyrene absorption can be a convenient method for probing critical micellar concentration (cmc) and indexing micellar polarity. *J. Colloid Interface Sci.* **2006,** 294, (1), 248-254.

57. Zhang, L.; Eisenberg, A., Multiple morphologies and characteristics of "crew-cut" micelle-like aggregates of polystyrene-b-poly (acrylic acid) diblock copolymers in aqueous solutions. *J. Am. Chem. Soc.* **1996,** 118, (13), 3168-3181.

58. Matyjaszewski, K., Controlled radical polymerization. *Curr. Opin. Solid State Mater. Sci.* **1996,** 1, (6), 769.

59. Lunt, S. Y.; Vander Heiden, M. G., Aerobic glycolysis: meeting the metabolic requirements of cell proliferation. *Annu. Rev. Cell Dev. Biol.* **2011,** 27, 441-464.

60. Planche, T.; Krishna, S., Severe malaria: metabolic complications. *Curr. Mol. Med.* **2006,** 6, (2), 141-153.

61. Loll, P. J.; Upton, E. C.; Nahoum, V.; Economou, N. J.; Cocklin, S., The high resolution structure of tyrocidine A reveals an amphipathic dimer. *Biochim. Biophys. Acta* **2014,** 1838, (5), 1199.

62. Munyuki, G.; Jackson, G. E.; Venter, G. A.; Kövér, K. E.; Szilágyi, L.; Rautenbach, M.; Spathelf, B. M.; Bhattacharya, B.; van der Spoel, D., β-Sheet Structures and Dimer Models of the Two Major Tyrocidines, Antimicrobial Peptides from Bacillus aneurinolyticus. *Biochem. J.* **2013,** 52, (44), 7798.

63. Ismail, M.; Du, Y.; Ling, L.; Li, X., Artesunate-heparin conjugate based nanocapsules with improved pharmacokinetics to combat malaria. *Int. J. Pharm.* **2019,** 562, 162.

64. Jiang, W.; Kim, B. Y. S.; Rutka, J. T.; Chan, W. C. W., Nanoparticle-mediated cellular response is size-dependent. *Nat. Nanotechnol.* **2008,** 3, 145.

65. Oeuvray, C.; Bouharoun-Tayoun, H.; Gras-Masse, H.; Bottius, E.; Kaidoh, T.; Aikawa, M.; Filgueira, M.-C.; Tartar, A.; Druilhe, P., Merozoite surface protein-3: a malaria protein inducing antibodies that promote Plasmodium falciparum killing by cooperation with blood monocytes. *Blood* **1994,** 84, 1594-1602.

66. Bannister, L.; Butcher, G.; Dennis, E.; Mitchell, G., Structure and invasive behaviour of Plasmodium knowlesi merozoites in vitro. *Parasitology* **1975,** 71, (3), 483-491.

67. Bannister, L. H.; Hopkins, J. M.; Fowler, R. E.; Krishna, S.; Mitchell, G. H., A Brief Illustrated Guide to the Ultrastructure of Plasmodium falciparum Asexual Blood Stages. *Parasitol. Today* **2000,** 16, (10), 427-433.

68. Koch, M.; Baum, J., The mechanics of malaria parasite invasion of the human erythrocyte–towards a reassessment of the host cell contribution. *Cell. Microbiol.* **2016,** 18, (3), 319-329.

TABLE OF CONTENTS GRAPHIC

Poly(*N*-vinylpyrrolidone) anti-malaria conjugates of membrane disruptive peptides.

Simbarashe Jokonya [†], Marvin Langlais [†], Meta Leshabane[§], Paul W Reader [†], Johan A Vosloo [‡], Rueben Pfukwa [†], Dina Coertzen[§], Lyn-Marie Birkholtz[§], Marina Rautenbach[‡] and Bert Klumperman[†]**